Antimicrobial Activities of Green Biosynthesized Iron Oxide Nanoparticles Using *F. Carica* Fruit Extract

Nada Khudair Abbas[1], Azhar A. F. Al- Attraqchi[2], Jenan Hussien Taha[3]

[1] Prof. Department of physics, College of Science, University of Baghdad, Baghdad, Iraq, [2]Prof. Department of Microbiology, College of Medicine, University of Al- Nahrain, Baghdad, Iraq, [3] Tutor, Physiology and Medical Physics Department, College of Medicine, University of Al- Nahrain, Baghdad, Iraq

Abstract

In the current study, iron oxide nanoparticles (IO NPs) were synthesized via modified green synthesis technique using *F. carica* fig extract as reducing agent. Furthermore, the microstructural properties of the synthesized IO NPs have been thoroughly elucidated. In details, the acquired NPs diameter was found to be in the range of 11-29 nm and of root mean square (RMS) of 0.64 nm using TEM and AFM techniques, respectively. Consequently, the antifungal and antibacterial activities of the synthesized IO NPs were screened against *Candida* and *Aspergillus* species as well as Gram-positive *Staphylococcus aureus* and Gram-negative *Acinetobacter* species, respectively. The presented IO NPs play an active role in the antimicrobial activities evidencing the well-organized materials system for biomedical applications.

Keywords: *Iron oxide NPs, antifungal, antibacterial, F. carica extract*

Introduction

Metal oxide NPs are of great importance due to a number of unique properties such as high surface-to-volume ratio, easy separation features, and low toxicity [(1)]. IO NPs have attracted a great significance in the field of nanoscience and nanotechnology [(2, 3)]. In conjunction with IO NPs, several applications have been proposed in the area of optoelectronics, catalysis, self-powered smart window, lithium ion batteries and diagnostic biological probes [(4-8)]. IO NPs are extensively applied in the biomedicine field due to their low toxicity and biocompatibility. Due to the electrostatic feature of the IO NPs, they are easily interact with fungal, and bacterial living-cell membranes [(9)]. This property allows IO NPs to harms the cell membranes of fungi or bacteria as well as inducing the toxic oxidative stress via free radical formation [(10)]. Antimicrobial activities of IO NPs are, therefore, dependent on three essential features namely concentration of the culture media and most importantly stability [(9, 10)].

Corresponding author:
Jenan Hussien Taha
asjenan@gmail.com

In this attempt, variety of approaches have been anticipated for the synthesis of IO NPs. Among these are the well-known physical and chemical methods in which preferred NPs properties can be acquired. Particularly, these methods are electrodeposition [(11)], conventional heating [(12)], hydrothermal [(13, 14)], wet oxidation [(15)], laser ablation [(16)], co-precipitation [(17, 18)], and anodization [(19)]. However, these techniques are presented with several draw-backs such as the use of non-biodegradable stabilizing agents and toxic chemicals, and hypothetically harmful to the well-being organisms and the surrounding environment. The green synthesis technique, which is utilized in the current study, has revealed considerable advances such as environmentally friendly, unpresented toxic chemicals, and low energy and temperature conditions [(20)]. Green synthesis technique evolves the use of naturally existing resources such as plants extracts as reducing fuel [(21)]. Therefore, this manuscript reports a modified green synthesis technique of IO NPs in which *F. carica* fig extract is used as a reducing agent. Additionally, the antifungal activity against *Candida* and *Aspergillus* species and antibacterial activity against Gram-positive *S. aureus* and Gram-negative *Acinetobacter* species were thoroughly investigated.

Materials and Methods

Plant collection and extraction

Dried *F. carica* (common fig) was purchased from local market in Baghdad, Iraq. Consequently, the collected fruit was washed thoroughly; afterward, 10 gm of the washed fruit was blended alongside 150 mL of deionized-distilled water (DDW). The resultant mixture was subjected to heating process at 100 °C in a ventilation oven and then cooled down to room temperature. Finally, the solution mixture was filtered using chromatography paper (Whatman No.1) and incubated at room temperature for further use.

Synthesis of IO NPs

In a typical laboratory route, specific amount (0.1, 0.14 and 0.18 molar) of iron^{III} chloride hexahydrate ($F_2Cl_3.6H_2O$) was liquefied in 100 mL of DDW under stirring rate of 800 r.p.m. for 15 minutes at RT. The consequential mixture was then mixed with fig extract (1:1) under stirring rate of 600 r.p.m. for 2 h at 50 °C [(1)]. The first indication of the NPs occurring was observed upon color changing of the solution, whereby a light brown color was noticed, as presented in figure (1). The acquired solution was then washed and centrifuged at 4000 r.p.m. for 20 minutes. Hereinafter, the attained residual was dried for 6 h at 60 °C and later grinded using mortar and pestle to obtain a fine NPs powder.

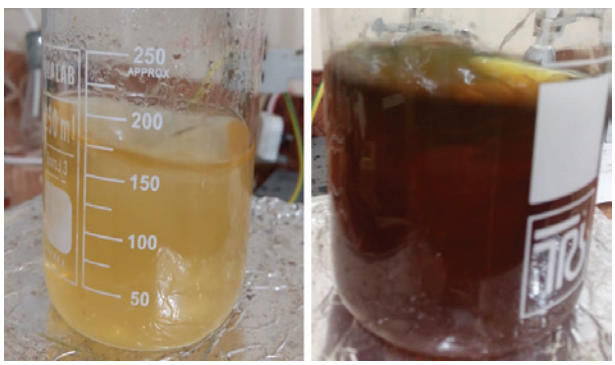

Figure (1): Color changing process of IO NPs.

Characterization

The microstructural properties of the prepared NPs were examined using Shimadzu X-ray Diffractometer (XRD-6000) with wavelength of 1.541 A° and Cu-Kα radiation. In the meanwhile, compact char surface was investigated using Fourier Transform Infrared Spectroscopy (FT-IR, Thermo Nicolet Nexus) ranging from 400 to 4000 cm^{-1}. Furthermore, the optical properties of the prepared NPs were recorded on Shimadzu UV-1800 UV-Vis spectrophotometer. Atomic Force Microscopy (SPM AA3000-AFM) and TECNAI F-30 TEM were engaged for the morphological and nanoparticle size investigations.

Evaluation of antifungal and antibacterial activities

The antifungal activity of the synthesized NPs was monitored using agar well diffusion procedure against two fungal species which are *Candida* and *Aspergillus* species [(22)]. Agar petri dish, which was used in this study as a culture media holder, was systematically swabbed with sterile cotton swab in which a 30 ml of 24 h Sabouraud′s dextrose was used for each fungal species. Continuously, wells were made in the pre-solidified agar plates with the help of 5 mm cork bor-er. Variety of the synthesized NPs concentrations (0.75, 1.5, 3, 6, 12 and 24 mg/ml) were sonicated with DDW and then used to evaluate the antifungal activity. Concurrently, Negative and positive control against the fungal pathogens was exhibited using DDW and antibiotics. Hereinafter, the cultured agar plates were incubated at 35 °C for 48 h, while the inhibition zones were measured in millimeter.

As for the IO NPs antibacterial activity, similar route to the aforementioned antifungal was repeated. However, the antibacterial activity was screened against Gram-positive *S. aureus* and Gram-negative *Acinetobacter* species using 30 ml of 24 h Blood agar culture media. In this experiment, the positive and negative controls used were antibiotics and DDW and the antibacterial activity was later proceeded to an incubation procedure for 24 h at 35℃. It is worth mentioning that the concentrations of IO NPs utilized for the antibacterial activity are 0.5, 1, 2, 4, and 8 mg/ml.

Results and Discussion

The XRD patterns of the synthesized NPs are presented in figure (2, a). Generally, the intensity of the diffraction peaks augmented with increasing IO NPs concentrations which in turn indicates higher crystallinity at high concentrations. As depicted in the figure, eight different pronounced peaks were acquired corresponding to (110), (120), (211), (10-1), (202), (211), (312), and (310) planes and diffraction angle of 2θ = 21.9°, 26.6°, 33.2°, 35.6°, 49.5°, 50.4°, 54°, and

62.4°, respectively (Card No. 96-901-1413) [1]. The (110), (120), and (211) planes mainly belong to FeO_2 phase, while other planes, (211), (10-1), (202), (312), and (310), are corresponded to Fe_2O_3 phase (Card No. 96-900-9783) [9].

Figure (2, b) illustrates the FT-IR curve of the synthesized NPs with concentration of 0.14 M. It is clear to be noticed that characteristic peaks at 3848, 3737, and 3416 cm^{-1} are mainly attributed to the O-H stretching bonds. In the meanwhile, peak at around 2925, cm^{-1} is corresponded to C-H stretching characteristic. Two pronounced peaks at 2381, and 2310 cm^{-1} are designated to O=C=O stretching. Furthermore, additional peaks at 1737, and 1638 cm^{-1} were observed which are due to C=O stretching, while peak at 1542 cm-1 is found to be in accordance with C=C stretching [1, 23]. Finally, Fe-O vibrations namely 1098, 795, 506 and 463 cm^{-1} are assigned to the IO NPs [23].

The UV-vis spectra of the synthesized IO NPs are demonstrated in figure (2, c), which exhibited broad bands and cut-off phenomenon at 360 nm. Furthermore, as illustrated in the figure, there is a decrease in the mentioned phenomenon cut-off towards higher wavelength as the concentration enlarged; this could be attributed to the lattice defects in the prepared NPs matrix [9].

Figure (2, d) demonstrates two dimensions and three dimensions AFM images of the synthesized NPs with a concentration of 0.14 M and scanning area of 2 µm. In general, the formed NPs exhibited a vertically aligned NPs with regular spherical shape and homogenous distribution. The average diameter and RMS were found to be 84.4 and 0.64 nm, respectively. In the meanwhile, the average surface roughness was found to be 0.54 nm; this indicates a pronounced rough surface which in turn reveals high electrochemical performance [24].

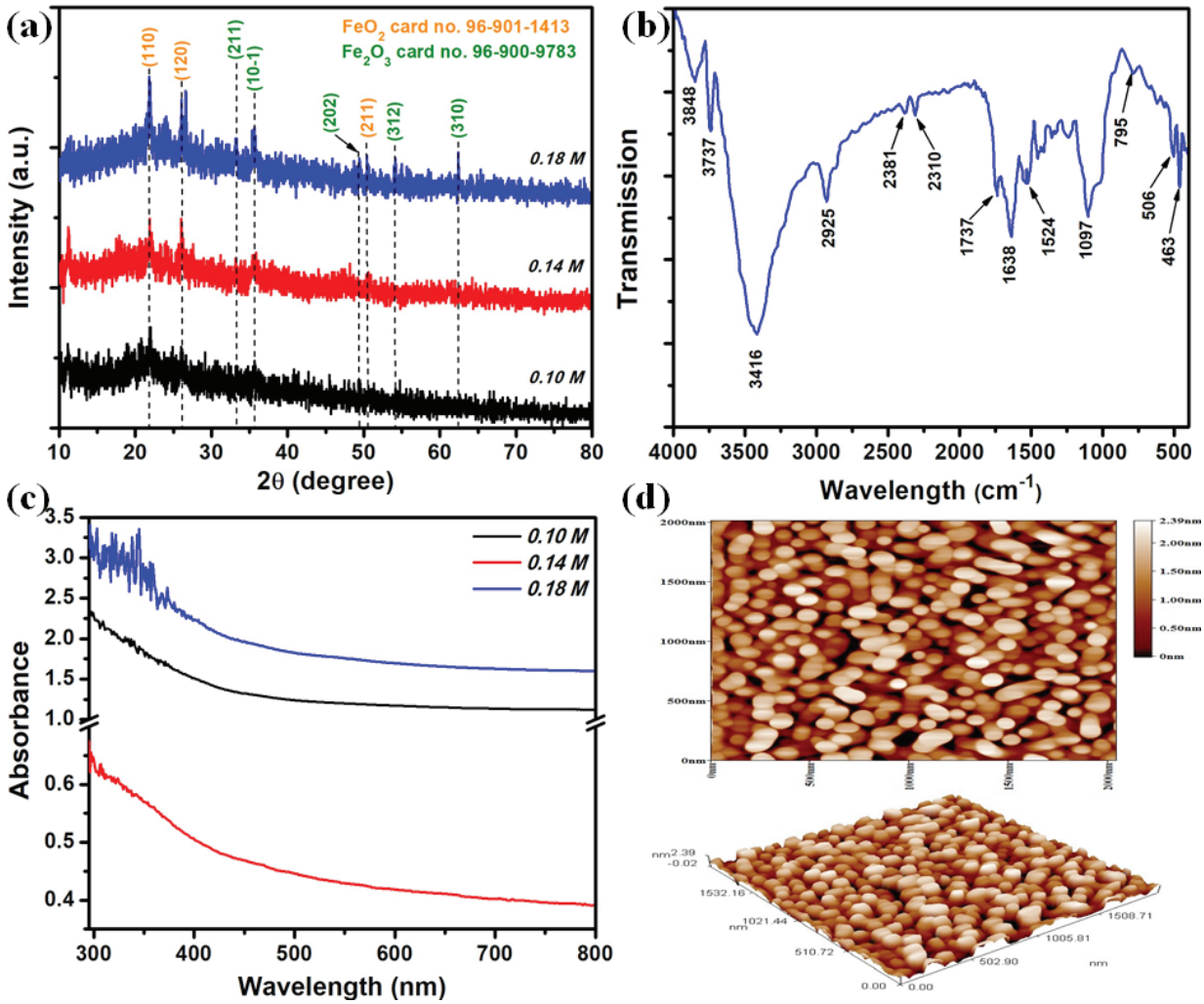

Figure (2): (a) XRD patterns, (b) FT-IR spectra, (c) UV-vis spectra, and (d) AFM of 2D and 3D images of the prepared NPs.

The TEM image of IO NPs is presented in figure (3, a and b). Generally, the synthesized NPs revealed almost a spherical structure with average diameter of 19 nm. From the figure, it also can be observed that a uniform IO NPs distribution which found to be in good agreement with the AFM findings. Furthermore, figure (3, b) shows the NPs diameter distribution which was found to be in the range of 11-29 nm.

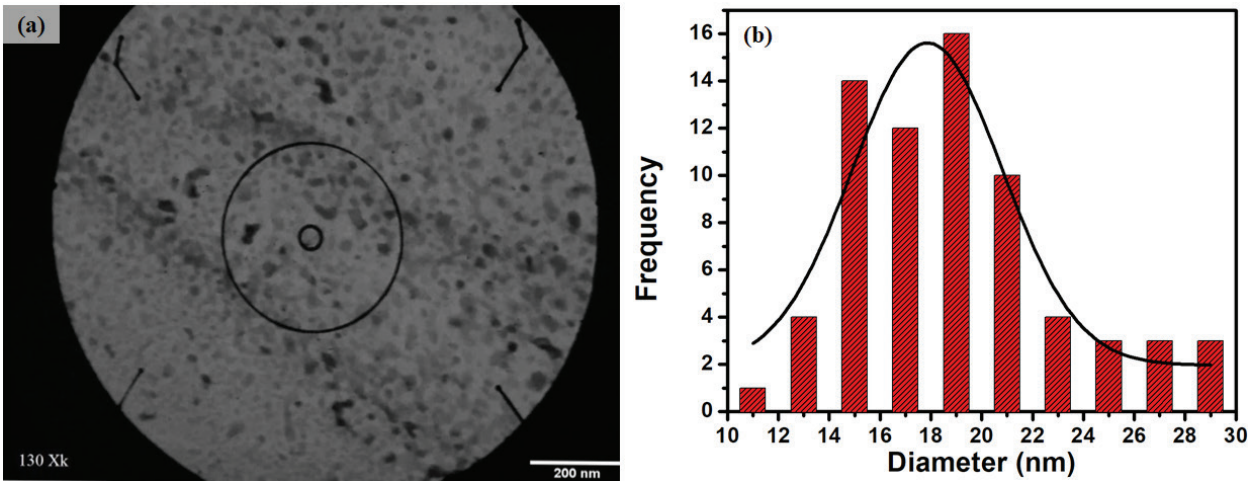

Figure (3): IO NPs with 0.14 M concentration (a) TEM image (b) diameter range distribution.

The antifungal activity of the green synthesized NPs against *Candida* and *Aspergillus* species are shown in figure (4, a). As presented in the figure, an observable inhibition zone increment in both kind of fungi species can be clearly seen as the concentration of the IO NPs increased, this indicates the active role of the synthesized NPs as an antifungal. This can be explained by the superior features of IO NPs such as large surface area, and small particle size as compared to their bulk nature [25]. Although, the inhibition zones in the case of *Candida* demonstrated larger inhibition diameter, lower concentrations of the used NPs were found to be active in the case of *Aspergillus*. The maximum inhibition zone diameters were found by the highest IO NPs concentration 24 (mg/ml) against *Candida* (35 mm) followed by *Aspergillus* (33 mm). In contrast, inhibition zone diameters of 10 and 15 mm against *Candida* and *Aspergillus* with IO NPs concentration of 3 mg/ml, respectively. Similarly, at concentration of 1.5 mg/ml, the antifungal activity was only exhibited against *Aspergillus*. This may be due the differences in the *Candida* species' cell wall structure which consists of high chitin as a yeast as compared to the moldy in *Aspergillus* species [26], this in turn leads to different sub-capability of each towards the tested nanoparticles.

Figure (4, b) presents the antibacterial activity of IO NPs against Gram-positive *S. aureus* and Gram-negative *Acinetobacter* species. Generally, increasing the concentration of IO NPs exhibited higher antibacterial activity. This could be attributed to the metallic NPs accumulation in the living cell-membranes which in turn releases cellular compounds as previously reported by other researchers [27]. It is a necessity to be stated that concentration as low as 0.5 mg/ml exhibited null activity against both species. However, higher concentrations of IO NPs displayed advanced inhibition zones in both species cases. Continuously, the acquired inhibition zones against Gram-negative *Acinetobacter* bring about more diameter range as compared to Gram-positive *S. aureus* at all concentrations. Inhibition zones of 25 and 19 mm in diameter against Gram-negative *Acinetobacter* and Gram-positive *S. aureus* were screened with IO NPs concentration of 8 mg/ml, respectively. This may be due to the difference in susceptibilities property of each bacterial species towards IO nanoparticles comes from the differences in the structure of cell wall of each bacteria. In details, the Gram-positive *S. aureus* species has thicker peptidoglycan and thus demonstrate higher resistance in contrast to Gram-negative *Acinetobacter*. As observed in table (1 and 2), the synthesized NPs

2866

dem

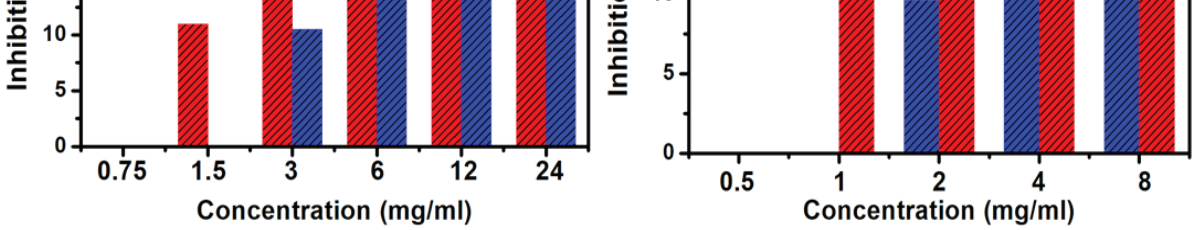

Figure (4): Inhibition zones of IO NPs; (a) fungi and (b) bacteria.

Table (1): Antibiotics zone of inhibition diameters against fungi.

fungal	inhibition zone (mm)				
	KCA (10 µg)	NY (100un)	AMB (20µg)	FCN (10µg)	DDW
candida spp.	34	14	11.4	22	0
Aspergillus spp.	21	16	12	0	0

Table (2): Antibiotics zone of inhibition against bacteria.

bacterial	inhibition zone (mm)							
	CRO (30 µg)	AK (30µg)	SAM (20µg)	TS (25µg)	CD (2µg)	CIP (5µg)	ATH (15µg)	DDW
S. aureus	26	17.5	14.5	13.5	0	0	0	0
Acinetobacter baumanii	0	0	0	0	0	0	0	0

Conclusion

IO NPs were successfully synthesized using *F. carica* fig extract. Additionally, the microstructural properties of the prepared NPs were illustrated using XRD, FT-IR, UV-vis, AFM and TEM techniques. Simultaneously, the synthesized NPs were evaluated for their antifungal and antibacterial activities against *Candida* and *Aspergillus* species as well as *S. aureus* and *Acinetobacter* species, respectively. It was found that *Aspergillus* species is more sensitive to the synthesized NPs rather than *S. aureus,* shedding the light towards this technique which may be useful for the treatment of this aggressive multidrug resistant bacteria.

Ethical Clearance: The Research Ethical Committee at scientific research by ethical approval of both MOH and MOHSER in Iraq

Conflict of Interest: Non

Funding: Self-funding

References

1. Demirezen DA, Yıldız YŞ, Yılmaz Ş, Yılmaz DD. Green synthesis and characterization of iron oxide nanoparticles using Ficus carica (common fig) dried fruit extract. Journal of bioscience and bioengineering. 2019;127(2):241-5.
2. Naseem T, Farrukh MA. Antibacterial activity of green synthesis of iron nanoparticles using Lawsonia inermis and Gardenia jasminoides leaves extract. Journal of Chemistry. 2015;2015.
3. Salih EY, Sabri MFM, Hussein MZ, Sulaiman

K, Said SM, Saifullah B, et al. Structural, optical and electrical properties of ZnO/ZnAl 2 O 4 nanocomposites prepared via thermal reduction approach. Journal of Materials Science. 2018;53(1):581-90.

4. Kouhbanani MAJ, Beheshtkhoo N, Taghizadeh S, Amani AM, Alimardani V. One-step green synthesis and characterization of iron oxide nanoparticles using aqueous leaf extract of Teucrium polium and their catalytic application in dye degradation. Advances in Natural Sciences: Nanoscience and Nanotechnology. 2019;10(1):015007.
5. Aslam MK, Shah SSA, Najam T, Li S, Chen C. Decoration of cobalt/iron oxide nanoparticles on N-doped carbon nanosheets: Electrochemical performances for lithium-ion batteries. Journal of Applied Electrochemistry. 2019;49(4):433-42.
6. Swidan MM, Khowessah OM, El-Motaleb MA, El-Bary AA, El-Kolaly MT, Sakr TM. Iron oxide nanoparticulate system as a cornerstone in the effective delivery of Tc-99 m radionuclide: a potential molecular imaging probe for tumor diagnosis. DARU Journal of Pharmaceutical Sciences. 2019;27(1):49-58.
7. Salih EY, Sabri MFM, Tan ST, Sulaiman K, Hussein MZ, Said SM, et al. Preparation and characterization of ZnO/ZnAl 2 O 4-mixed metal oxides for dye-sensitized photodetector using Zn/Al-layered double hydroxide as precursor. Journal of Nanoparticle Research. 2019;21(3):55.
8. Bashir MBA, Said SM, Sabri MFM, Miyazaki Y, Shnawah DA, Shimada M, et al. In-Filled La 0.5 Co 4 Sb 12 Skutterudite System with High Thermoelectric Figure of Merit. Journal of Electronic Materials. 2018;47(4):2429-38.
9. Ismail RA, Sulaiman GM, Abdulrahman SA, Marzoog TR. Antibacterial activity of magnetic iron oxide nanoparticles synthesized by laser ablation in liquid. Materials Science and Engineering: C. 2015;53:286-97.
10. Iwamoto T, Ishigaki T, editors. Fabrication of iron oxide nanoparticles using laser ablation in liquids. Journal of Physics: Conference Series; 2013: IOP Publishing.
11. Aghazadeh M, Karimzadeh I. One-pot electro-synthesis and characterization of chitosan capped superparamagnetic Iron oxide nanoparticles (SPIONs) from ethanol media. Current Nanoscience. 2018;14(1):42-9.
12. Zhu J, Yang Z, Li X, Qi S, Jia M. Application of microwave heating with iron oxide nanoparticles in the in□situ exploitation of oil shale. Energy Science & Engineering. 2018;6(5):548-62.
13. Pandi K, Viswanathan N, Meenakshi S. Hydrothermal synthesis of magnetic iron oxide encrusted hydrocalumite-chitosan composite for defluoridation studies. International journal of biological macromolecules. 2019;132:600-5.
14. John Vagabond's Physics and Chemistry Blog. HOW DO PHOTONS INTERACT WITH MATTER? SIMPLE SCATTER, COMPTON SCATTER, PAIR PRODUCTION 2014, April 14. Available from: https://johnvagabondscience.wordpress.com/tag/pair-production/.
15. Elnabawy HM, Casanova-Chafer J, Anis B, Fedawy M, Scardamaglia M, Bittencourt C, et al. Wet chemistry route for the decoration of carbon nanotubes with iron oxide nanoparticles for gas sensing. Beilstein journal of nanotechnology. 2019;10(1):105-18.
16. Zhang D, Choi W, Oshima Y, Wiedwald U, Cho S-H, Lin H-P, et al. Magnetic Nanoblends Fe@ FeO Synthesized x Single-Crystal by Femtosecond Laser Ablation of Fe in Acetone. Laser-Based Nano Fabrication and Nano Lithography. 2018:107.
17. Salih EY, Abbas Z, Al Ali SHH, Hussein MZ. Dielectric behaviour of Zn/Al-NO3 LDHs filled with polyvinyl chloride composite at low microwave frequencies. Advances in Materials Science and Engineering. 2014;2014.
18. Salih EY, Sabri MFM, Sulaiman K, Hussein MZ, Said SM, Usop R, et al. Thermal, structural, textural and optical properties of ZnO/ZnAl2O4 mixed metal oxide-based Zn/Al layered double hydroxide. Materials Research Express. 2018;5(11):116202.
19. Lucas-Granados B, Sánchez-Tovar R, Fernández-Domene RM, Garcia-Anton J. Influence of electrolyte temperature on the synthesis of iron oxide nanostructures by electrochemical anodization for water splitting. International Journal of Hydrogen Energy. 2018;43(16):7923-37.
20. Kavitha K, Baker S, Rakshith D, Kavitha H, Yashwantha Rao H, Harini B, et al. Plants as green source towards synthesis of nanoparticles. Int Res J Biol Sci. 2013;2(6):66-76.

21. Groiss S, Selvaraj R, Varadavenkatesan T, Vinayagam R. Structural characterization, antibacterial and catalytic effect of iron oxide nanoparticles synthesised using the leaf extract of Cynometra ramiflora. Journal of Molecular Structure. 2017;1128:572-8.
22. Pérez Rodríguez C, Paul M, Bazerque P, Perez-Eid C. An Antibiotic assay by the agar well diffusion method. 1990.
23. Namduri H, Nasrazadani S. Quantitative analysis of iron oxides using Fourier transform infrared spectrophotometry. Corrosion Science. 2008;50(9):2493-7.
24. Soomro RA, Sherazi SH, Memon N, Shah M, Kalwar N, Hallam KR, et al. Synthesis of air stable copper nanoparticles and their use in catalysis. Adv Mater Lett. 2014;5(4):191-8.
25. Khan I, Saeed K, Khan I. Nanoparticles: Properties, applications and toxicities. Arabian Journal of Chemistry. 2019;12(7):908-31.
26. dos Santos VM, Dorner JW, Carreira F. Isolation and toxigenicity of Aspergillus fumigatus from moldy silage. Mycopathologia. 2003;156(2):133-8.
27. Sondi I, Salopek-Sondi B. Silver nanoparticles as antimicrobial agent: a case study on E. coli as a model for Gram-negative bacteria. Journal of colloid and interface science. 2004;275(1):177-82.